



ELSEVIER

Available online at www.sciencedirect.com

SCIENCE @ DIRECT®

Coastal Engineering 50 (2004) 139–159

**Coastal
Engineering**
An International Journal for Coastal,
Harbour and Offshore Engineers

www.elsevier.com/locate/coastaleng

Eddy viscosity and Eulerian drift over rippled beds in waves

François Marin*

Laboratoire de Mécanique, Physique et Géosciences, Université du Havre, Place Robert Schuman, B.P. 4006, 76610 Le Havre, France

Received 24 October 2002; received in revised form 4 September 2003; accepted 6 October 2003

Abstract

This paper reports the results of an experimental study of the Eulerian drift induced by weakly asymmetrical progressive waves in the bottom boundary layer over rippled beds in the transitional flow regime. Fourteen tests were carried out in a wave flume and one test in a steady flow flume for the estimation of the Nikuradse roughness length k_s of the artificial rippled bed which was used. The fluid velocities were measured with a two-component laser-Doppler anemometer. The edge of the bottom wave boundary layer is estimated to be located at one Nikuradse roughness length above the level midway between crest and trough of the ripples. Momentum transfer in this boundary layer is dominated by organized vortices. An analytical model based on a time-varying eddy viscosity was developed by Davies and Villaret [J. Geophys. Res. 104 (C1) (1999) 1465] for the estimation of the wave-induced Eulerian drift above rippled and very rough beds in the turbulent flow regime. Present data show that the applicability of this model can be extended to the “lower” part of the transitional flow regime in the parameter ranges $1000 \leq R \leq 6500$ and $1 \leq alk_s \leq 3$, where R is the flow Reynolds number and a is the orbital amplitude of fluid, if adjusted values of the model coefficients which represent the variation amplitude of the symmetrical and asymmetrical time-varying components of the eddy viscosity are used. The drift at the edge of the boundary layer is oriented in the direction of wave propagation in the transitional flow regime, while this drift is oriented in the opposite direction in the turbulent flow regime. The vertical profiles of Eulerian drift, horizontally averaged over a ripple length, are also compared with Longuet-Higgins’ [Philos. Trans. R. Soc. Lond., A 245(903) (1953) 535] solution for a laminar flow above a smooth bed and with Nielsen’s [Coastal bottom boundary layers and sediment transport. Advanced Series on Ocean Engineering, Vol. 4, World Scientific, Singapore, Chap. 1, pp. 40–60, 1992] solution involving a time-invariant eddy viscosity for turbulent flows over fairly rough beds.

© 2003 Elsevier B.V. All rights reserved.

Keywords: Bed ripples; Wave boundary layer; Waves; Eulerian drift; Eddy viscosity

1. Introduction

It is well known that water waves induce a steady streaming. Although this streaming is weak compared with the oscillatory component of velocity, it

has a significant effect on the transport of sediments and pollutants in the sea. This wave-induced current is due to the vertical velocities generated within the bottom boundary layer beneath progressive waves, which are not exactly out of phase with the horizontal velocities, leading to a nonzero time-averaged bed shear stress. Longuet-Higgins (1953) showed theoretically that, over a smooth flat bed in laminar

* Fax: +33-2-32-74-46-71.

E-mail address: francois.marin@univ-lehavre.fr (F. Marin).

flow, the Eulerian drift in the boundary layer at the bed is in the direction of wave propagation. Laboratory tests have shown good agreement between theory and experiment in this case (e.g., Collins, 1963; Brebner et al., 1966). Longuet-Higgins (1958) suggested that, subject to the assumption of a time- and height-invariant eddy viscosity ν_t , the drift at the edge of the boundary layer would be the same in turbulent flow as for laminar flow. Johns (1970) argued that this remains correct even if height variation is introduced into ν_t .

Sea beds are rarely smooth. Sleath (1974a) and Vittori and Blondeaux (1996) obtained small-perturbation solutions for the effect of bed roughness on the drift velocity. These solutions are limited to nonseparating flows. A numerical solution of the Navier–Stokes equations for separating flows over a rippled bed was proposed by Sleath (1974b). The influence of the waviness of the bed was found to depend on the Reynolds number and on the relative magnitude of the fundamental and the first harmonic in the flow outside the boundary layer. In the turbulent flow regime, the effect of bed roughness is to reduce the near-bed Eulerian drift. This results from a reduction of the phase lead of the bottom velocity in comparison with the lead of $\pi/4$ given by the classical Stokes' solution, as shown by Trowbridge and Madsen's (1984) two-layer eddy viscosity model. This behaviour which was observed qualitatively by Bijker et al. (1974) has also been obtained by Jacobs (1984), Brøker (1985) and O'Hare (1992). The approach used by Trowbridge and Madsen is particularly suitable for flows in which momentum transfer is dominated by turbulent processes, that is for $a/k_s \geq 30$, where a is the orbital amplitude of fluid at the edge of the boundary layer at the bed and k_s is the equivalent bed roughness. Nielsen (1992) suggested the use of a model based on a constant eddy viscosity for the estimation of the near-bed wave-induced currents for flows in the rough turbulent regime when $2 < a/k_s < 16.7$. The effect of asymmetry in the turbulence which was included in the models of Jacobs (1984), Trowbridge and Madsen (1984), Trowbridge et al. (1986) and Hsu and Ou (1994) was found under flat rough bed conditions, to reduce the near-bed Eulerian drift, with a reversal in the direction of drift occurring for very long waves. This effect of turbulence asymmetry has been demonstrated, in isolation from other processes, by Rib-

berink and Al-Salem (1995) in an oscillating water tunnel.

Davies and Villaret (1999) have developed an analytical model of the Eulerian drift induced by Stokes' second-order waves in the bottom boundary layer above rippled and very rough beds in the turbulent flow regime. In this case ($a/k_s \leq 5$), momentum transfer is dominated not by random turbulent processes, but by organized vortices which are shed from bed roughness elements at flow reversal. These authors adopted a one-dimensional, horizontally averaged description of the flow, based on a time-varying "convective" eddy viscosity. A one-dimensional approach does not allow a detailed description of the periodic vortex shedding process but has clear advantages for practical applications. This process can be represented by a two-dimensional hydrodynamic model (e.g., Block et al., 1994; Hansen et al., 1994; Huang and Dong, 2002). However, Scandura et al. (2000) mentioned that the breakdown of the two-dimensional vortices into smaller three-dimensional structures cannot be described assuming the flow to be two-dimensional. The solution obtained by Davies and Villaret (1999) for the Eulerian drift is characterized by a near-bed jet in the direction of wave advance, beneath a layer extending to the edge of the boundary layer in which the drift is in the opposite direction. The asymmetry terms arising from the time-varying components of the eddy viscosity cause the drift at the edge of the wave boundary layer to be in opposition to the wave direction, as measured by Van Doorn and Godefroy (1978), Villaret and Perrier (1992), Marin and Sleath (1994) and Mathisen and Madsen (1996b). Mathisen and Madsen (1996b) showed experimentally that the return current associated with a closed flume environment was very small at the edge of the wave boundary layer and that the drift observed at the edge of the boundary layer is the result of processes within the boundary layer.

Davies and Villaret (1998) pointed out that a very different behaviour is found in the transitional flow regime in comparison with the turbulent flow regime for the Eulerian drift induced by progressive waves in the bottom boundary layer above a rough bed. The purpose of the present study is to provide experimental data to improve the modelling of wave-induced currents in the bottom boundary layer above rippled

beds in the transitional flow regime and to make a contribution to bridge the gap between the model of turbulent flow developed by Davies and Villaret (1999) and the model of laminar flow presented by Longuet-Higgins (1953).

It should be kept in mind that the mass-transport velocity usually refers to the time-mean Lagrangian velocity which differs from the Eulerian drift considered in this paper. The present experiments have been carried out with fixed ripples. The presence of loose sand is likely to increase the turbulence intensity for a given ripple shape. This is contrary to what might be expected due to stabilisation by stratification but, nevertheless, is what was measured by Nakato et al. (1977). The effects of bed permeability have been investigated by Liu et al. (1996). The numerical results obtained by Huang and Dong (2002) show that a solitary wave above a rigid rippled bed induces a near-bed current in the opposite direction to that of the wave propagation.

2. Experimental set-up and test conditions

Fourteen tests were carried out in a wave flume for the study of wave-induced currents and one test was carried out in a steady flow flume for the estimation of the Nikuradse roughness length k_s of ripples.

2.1. Experimental equipment (waves experiments)

The experiments were carried out in a 9-m-long and 0.80-m-wide wave flume at the University of Le Havre. Progressive waves were produced by a piston type wave generator at one end of the flume and absorbed by a beach at the other end (Fig. 1a). In the test section, approximately 4.8 m from the wave generator, a set of 56 artificial ripples with a hydraulically smooth surface was located. The ripple profile (Fig. 1b) is described by the following parametric relationships:

$$x = \xi - \frac{\eta}{2} \sin\left(\frac{2\pi\xi}{\lambda}\right), \quad y = \frac{\eta}{2} \cos\left(\frac{2\pi\xi}{\lambda}\right) \quad (1)$$

where η is the ripple height ($\eta=3$ mm), λ is the wave length of the ripples ($\lambda=18$ mm), ξ is a dummy variable, and x and y the distances measured respectively in the horizontal and vertical directions. The origin of y is located at the level midway between crest and trough of the ripples. Longuet-Higgins (1953) mentioned that the flow in the bed boundary layer is determined by local conditions. Fredsøe et al. (1993) made an experimental study on the effects of a sudden change in bed roughness on wave boundary layers. They found that parameters such as bed shear

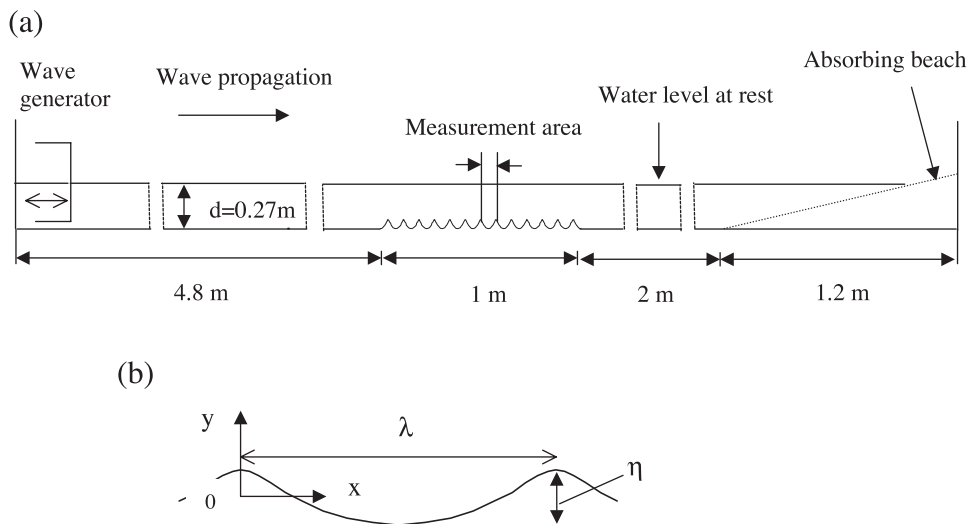


Fig. 1. (a) The flume. (b) The ripple geometry.

Table 1
Test conditions (waves experiments)

Test numbers	H (mm), wave height	U_∞ (m/s), near-bed velocity amplitude	R , wave Reynolds number	a/k_s , orbital- amplitude-to- equivalent-bed- roughness ratio (at bed)	B_{meas} , asymmetry parameter (measured values)	B_{th} , asymmetry parameter (theoretical values)
1	48	0.093	1487	1.34	0.028	0.026
2	92	0.176	5342	2.54	0.048	0.049
3	14	0.025	108	0.36		0.007
4	25	0.050	430	0.72	0.014	0.014
5	32	0.063	685	0.91	0.019	0.017
6	43	0.083	1190	1.20	0.026	0.023
7	52	0.101	1743	1.45	0.031	0.028
8	63	0.121	2496	1.74	0.035	0.033
9	74	0.140	3350	2.02	0.039	0.038
10	82	0.158	4264	2.28	0.042	0.043
11	91	0.177	5398	2.56	0.048	0.049
12	98	0.192	6309	2.76	0.051	0.053
13	107	0.207	7344	2.98	0.051	0.057
14	117	0.222	8441	3.20	0.079	0.061

stress were almost unaffected by a change in bed roughness at distances greater than a , the orbital amplitude of fluid, from the change in roughness. For present tests, the fluid velocities were measured near the bed at a distance from the upstream and downstream ends of the ripple patch corresponding at least to approximately $10a$. The limited length of the rippled bed is therefore unlikely to have affected the flow near the bed.

The fluid velocities were measured with a two-component, 4-W argon laser-Doppler anemometer in forward-scatter mode. The measurement volume was 0.14 mm^3 . At each measurement point, data acquisition was performed with a typical data rate of 6000 Hz during about 15 periods, which were split into 50 phases. The horizontal and vertical components of the instantaneous velocity (u, v) have been decomposed into periodic, phase-averaged components (u_p, v_p), and turbulent components (u', v'). In other words, we have for each phase: $u = u_p + u'$ and $v = v_p + v'$. For a rippled bed of wavelength λ , which is much smaller than the surface wavelength λ_s , the velocity components may be horizontally averaged locally (i.e., over one ripple wavelength) such that

$$u_p = \langle u_p \rangle + \tilde{u}_p, v_p = \langle v_p \rangle + \tilde{v}_p, \quad (2)$$

where

$$\langle u_p \rangle = \frac{1}{\lambda} \int_{x-\lambda/2}^{x+\lambda/2} u_p dx, \quad \langle v_p \rangle = \frac{1}{\lambda} \int_{x-\lambda/2}^{x+\lambda/2} v_p dx, \quad (3)$$

and \tilde{u}_p, \tilde{v}_p represent the variations in velocity occurring within one wavelength (with $\langle \tilde{u}_p \rangle = \langle \tilde{v}_p \rangle = 0$).

The test conditions are shown in Table 1. In this table, H is the wave height, U_∞ is the fundamental component of u_0 , the horizontal velocity just outside the boundary layer at the bed, R is the wave Reynolds number: $R = U_\infty a / \nu$, where ν is the kinematic viscosity and a is calculated by $a = U_\infty T / (2\pi)$, in which T is the wave period. The waves' asymmetry parameter B is defined by:

$$U_{\infty 2} = B U_\infty \quad (4)$$

in which $U_{\infty 2}$ is the amplitude of the second harmonic component of u_0 . In Table 1, U_∞ and B_{meas} were obtained by Fourier analysis of the velocity record u_0 , and B_{th} was calculated using the second-order Stokes wave theory:

$$B_{\text{th}} = \frac{0.75ka}{\sinh^2(kd)} \quad (5)$$

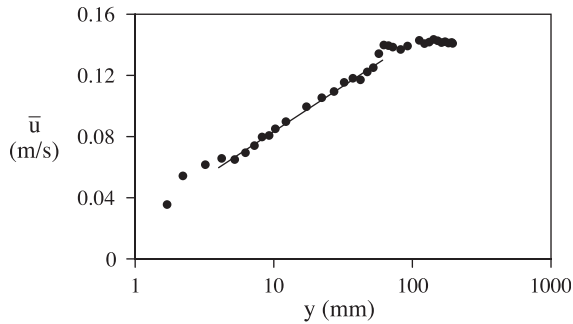


Fig. 2. Velocity profile above ripple crest in the case of current alone.

in which k is the surface wavenumber and d is the mean water depth. The agreement between theory and experiment is good, except for Test 14 where B_{meas} is 29.5% greater than B_{th} . This was due to the particularly large wave height for this test. For Test 3, $U_{\infty 2}$ was too weak to be measured. The present tests involve weakly asymmetrical waves ($B < 0.1$). The mean water depth was $d = 27$ cm and the wave period $T = 1.08$ s for all of the tests. In no test did wave breaking occur in the test section.

For Tests 1 and 2, the velocity measurements were carried out within a ripple wavelength, from the rippled bed up to approximately four ripple heights above the ripple trough level. Velocities were measured at about 600 measuring points for each one of these two tests. The grid spacing was 1 mm in the horizontal direction and 0.25–0.5 mm in the vertical direction. For Tests 3–14, the velocity measurements were carried out at one point at the edge of the bottom boundary layer, above the layer of influence of local topographic effects.

2.2. Estimation of the Nikuradse roughness length (current-alone experiment)

The Nikuradse roughness length k_s of ripples was estimated from one test carried out in a steady flow flume at the University of Le Havre. The test section of this flume is 3 m long and 0.30 m wide. The horizontal component of velocity can be written in the following way: $u = \bar{u} + u'$, \bar{u} being the time-mean value of u . The current flow rate provided a depth-averaged current velocity of 0.12 m/s in a water depth of 205 mm. The

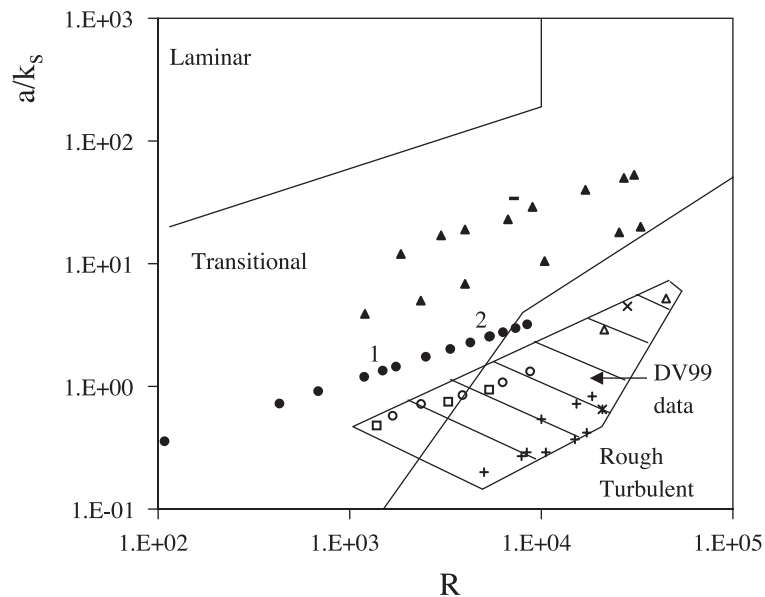


Fig. 3. Delineation of flow regimes proposed by Davies (1980), indicating the boundaries between laminar, transitional and rough turbulent oscillatory flow. The hatched area corresponds to the region of applicability of the Davies and Villaret's (1999) model. The symbols representing the data sets are as follows: solid triangles, Brebner et al. (1966); cross, Van Doorn and Godefroy (1978); open triangles, Villaret and Perrier (1992); dash, Klopman (1994); open squares, Marin and Sleath (1994); pluses, Mathisen and Madsen (1996b); asterisk, Fredsøe et al. (1999); open circles, Ridler and Sleath (2000); solid circles, present tests (Tests 1 and 2 are identified with the labels 1 and 2).

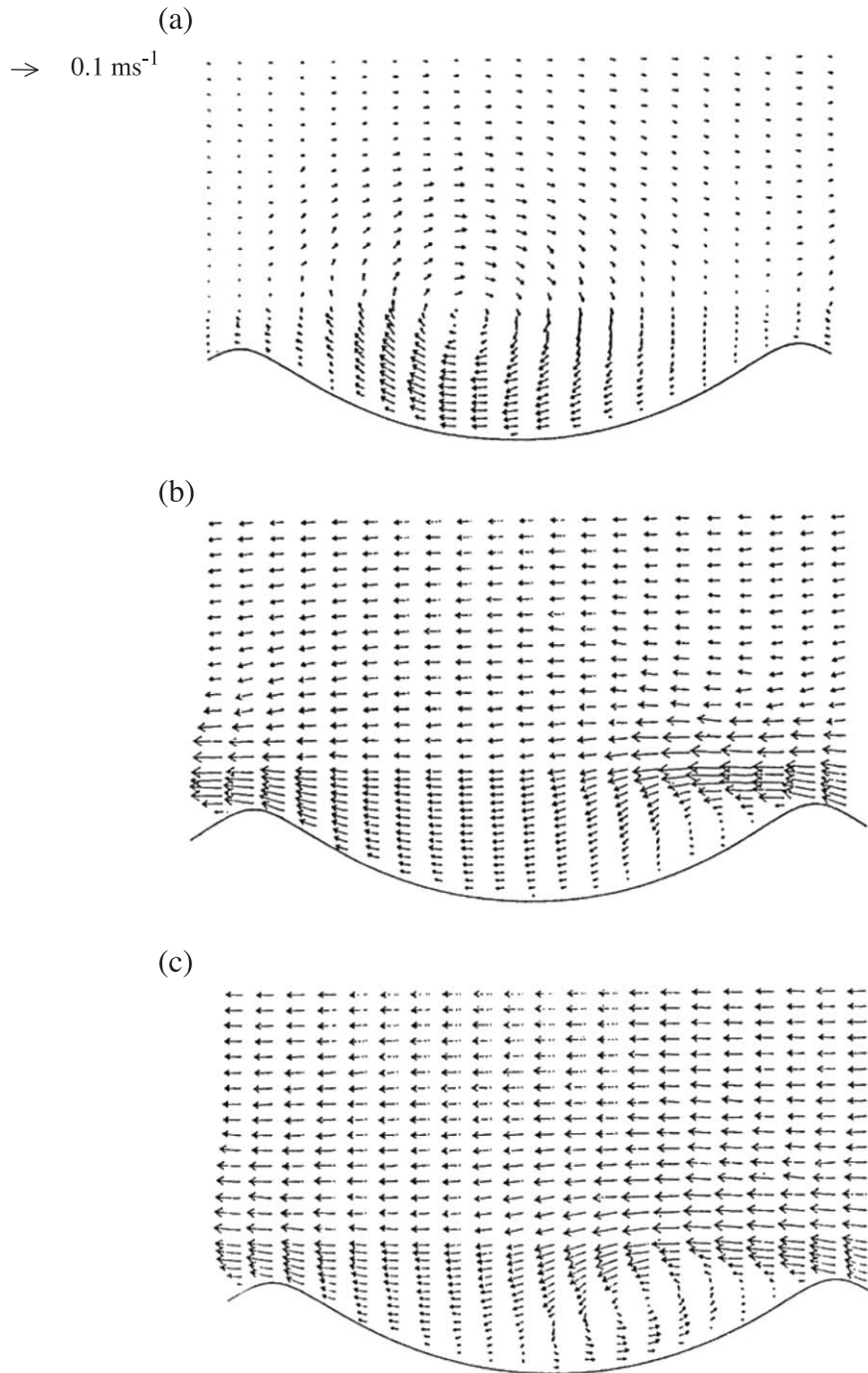


Fig. 4. Distributions of the periodic component of the velocity vector. Test 1. (a) $\omega t = 1.26$, (b) $\omega t = 2.26$, (c) $\omega t = 3.27$, (d) $\omega t = 4.27$, (e) $\omega t = 5.28$, (f) $\omega t = 6.28$.

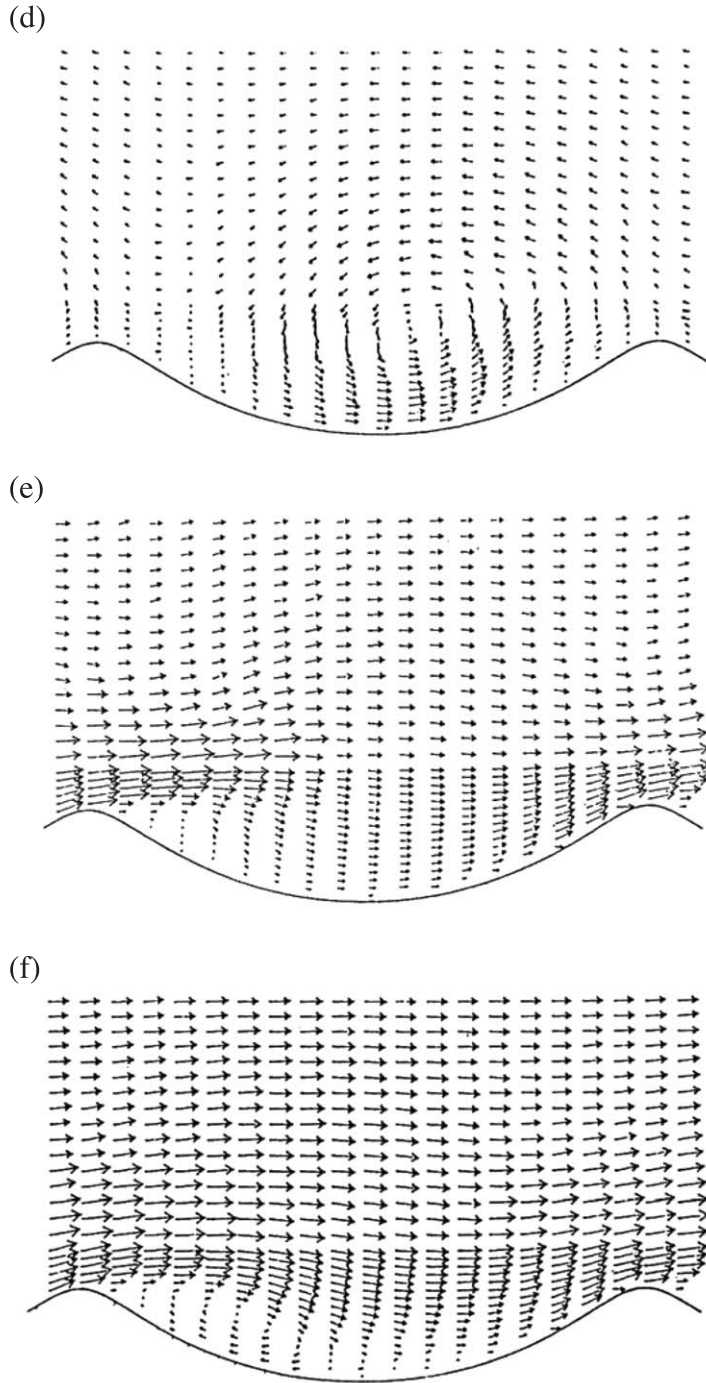


Fig. 4 (continued).

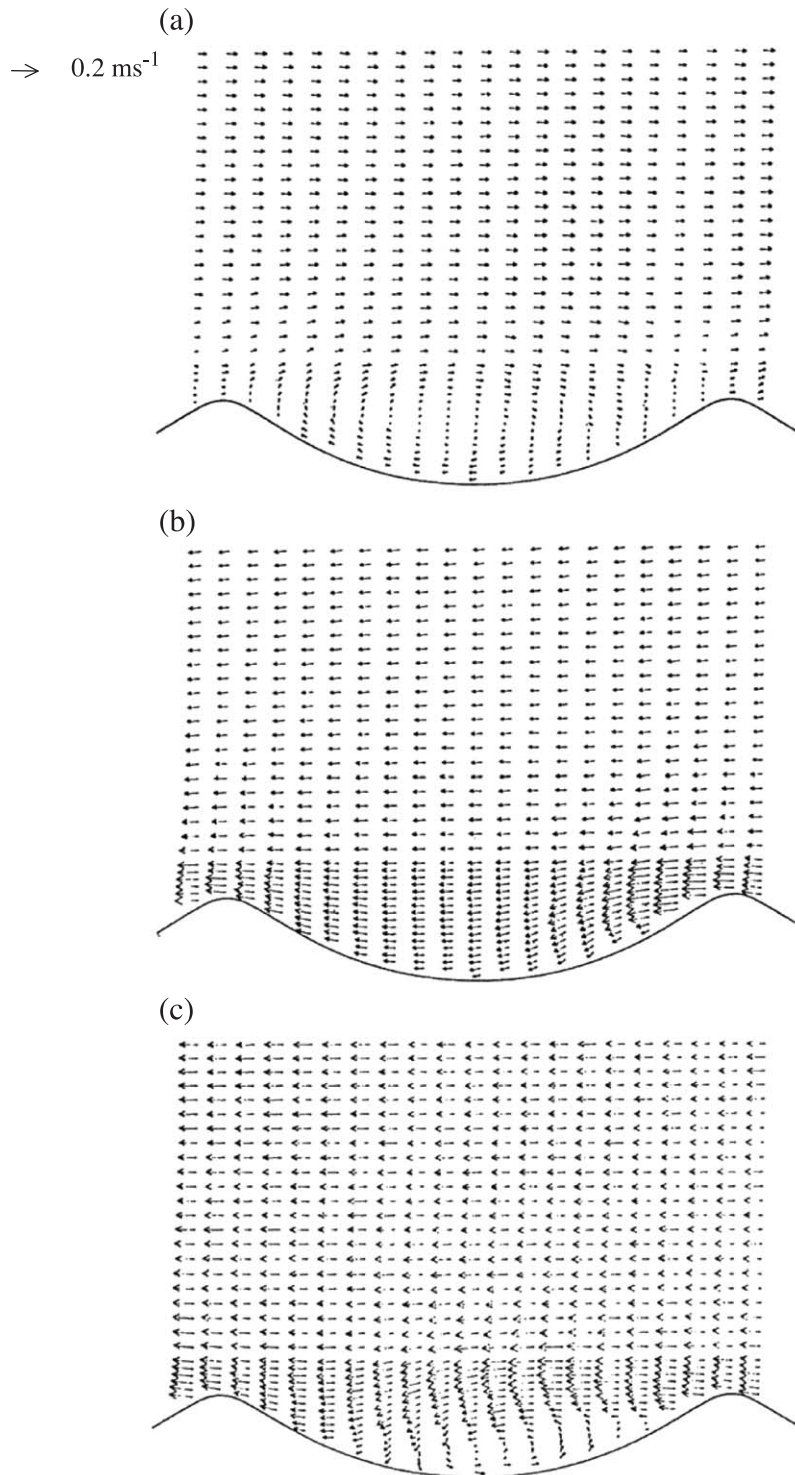


Fig. 5. Distributions of the periodic component of the velocity vector. Test 2. (a) $\omega t=1.01$, (b) $\omega t=2.01$, (c) $\omega t=3.02$, (d) $\omega t=4.02$, (e) $\omega t=5.03$, (f) $\omega t=6.03$.

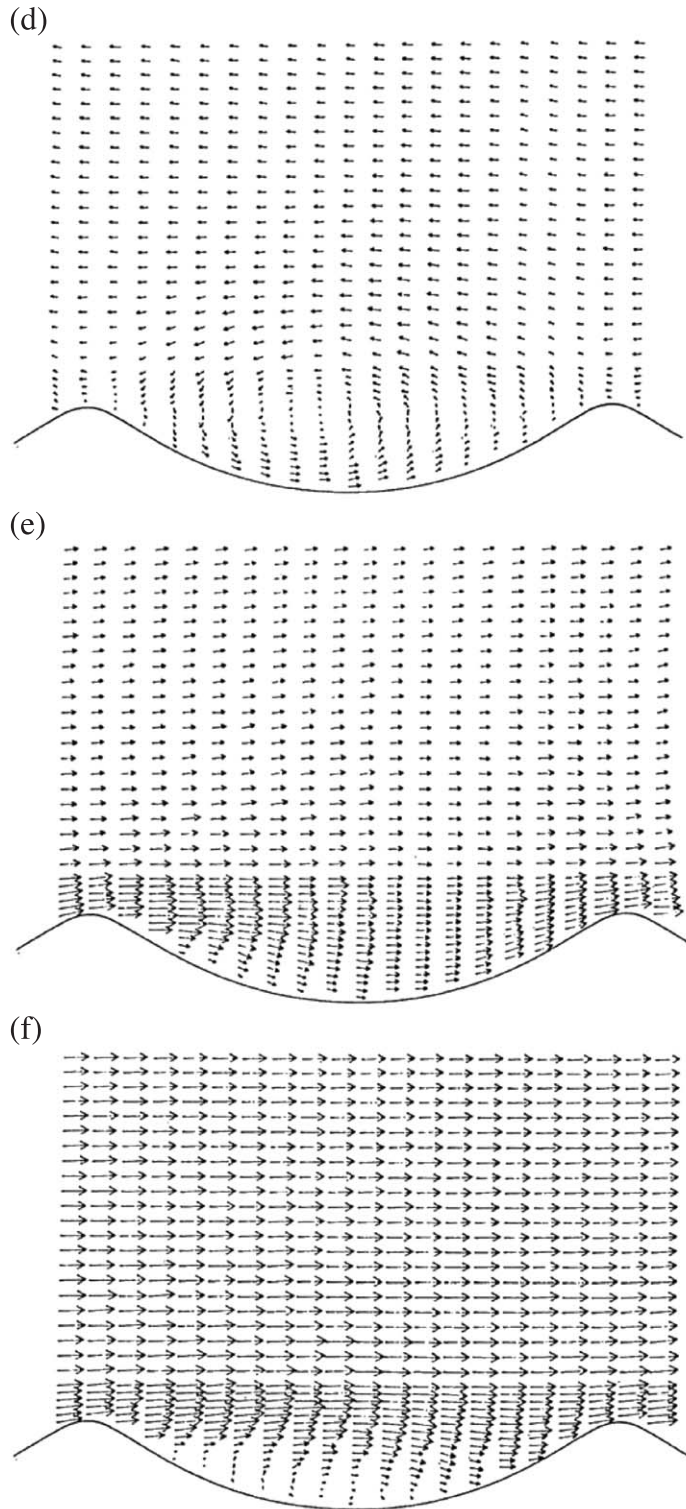


Fig. 5 (continued).

profile of \bar{u} above ripple crest is plotted in Fig. 2. For $5 < y < 50$ mm, the velocity profile can be described by a logarithmic law, characteristic of a turbulent flow. Mathisen and Madsen (1996a) mentioned that, for pure currents, the lower edge of the logarithmic region may be defined as one roughness element height above the tops of roughness elements. This is consistent with present data. One velocity profile has also been measured above ripple trough to ensure that the logarithmic velocity profile was not affected by the location of measurements with respect to the ripples. For $y > 50$ mm, the measurement points are in the outer flow. Consequently, the upper edge of the boundary layer is approximately 50 mm above the rippled bed. The best fit with the experimental data in the layer where the

velocity profile is logarithmic is given, using a least-squares technique, by the equation:

$$\bar{u} = 0.0258 \ln(y) + 0.0239 \quad (\text{for } 5 < y < 50 \text{ mm}), \quad (6)$$

where y is expressed in mm and \bar{u} in m/s. The time-mean shear velocity at bed \bar{u}^* can be estimated as 10.3 mm/s using the well-known Prandtl–Von Karman formula:

$$\bar{u} = \frac{\bar{u}^*}{K} \ln\left(\frac{y}{y_0}\right) \quad (7)$$

where $K = 0.4$ is the Karman constant and $y_0 = 0.40$ mm is the zero-intercept level of the logarithmic velocity

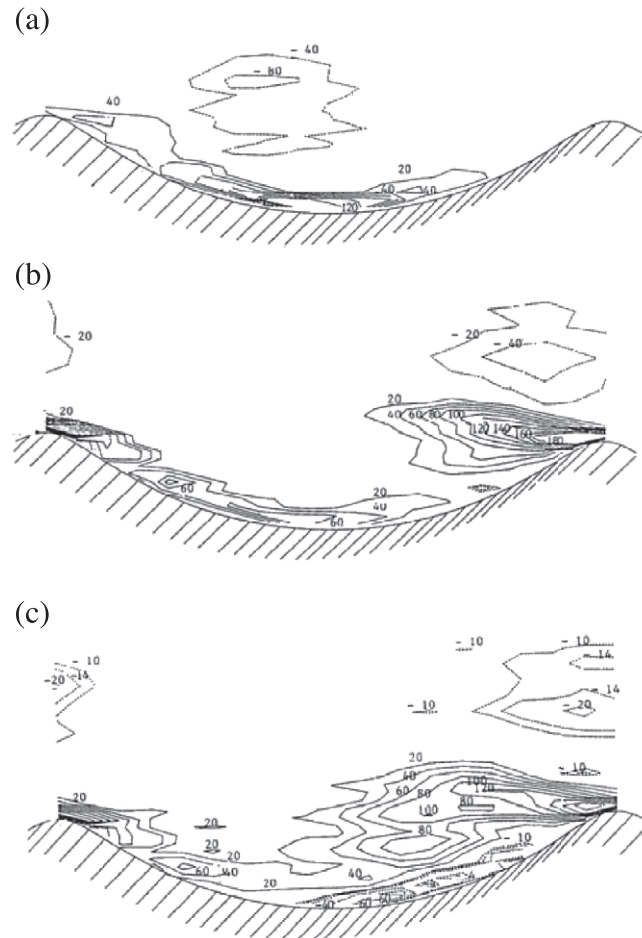


Fig. 6. Contours of the spanwise component of vorticity (rd/s). Test 1. (a) $\omega t = 1.26$, (b) $\omega t = 2.26$, (c) $\omega t = 3.27$, (d) $\omega t = 4.27$, (e) $\omega t = 5.28$, (f) $\omega t = 6.28$.

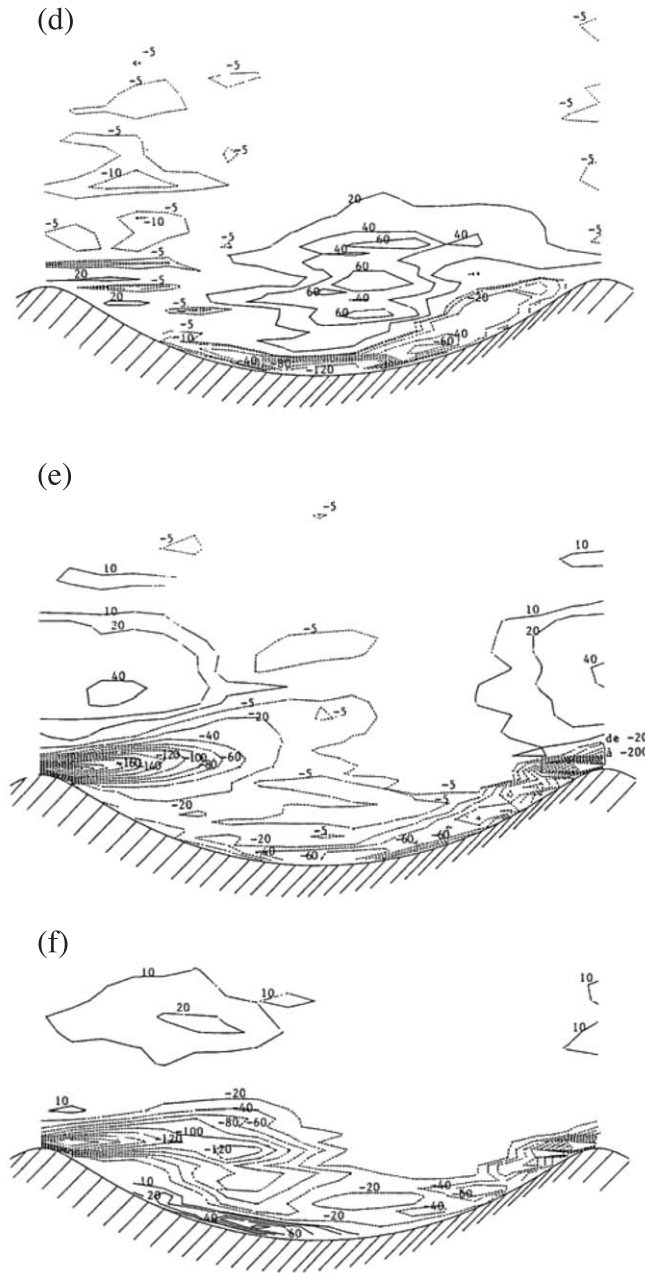


Fig. 6 (continued).

profile. The Nikuradse roughness length of the bed k_s can therefore be estimated as 11.9 mm using: $y_0/k_s = 1/30$, the equation which applies for turbulent boundary layers over hydraulically rough beds. The controlling parameter of the flow is the Reynolds number $R_* = \bar{u} * k_s /$

$\nu = 122 > 70$, the traditional value for the bed to be hydraulically rough. The value obtained for k_s is in good agreement with Swart's (1976) formula: $k_s = 25\eta^2/\lambda$, which leads to $k_s = 12.5$ mm. Mathisen and Madsen (1996a,b) concluded from their experi-

ments that the same value of k_s remains applicable in steady, oscillatory, and combined wave-current flow.

2.3. Flow regime (waves experiments)

The oscillatory boundary layer flow regimes proposed by Davies (1980) are shown in Fig. 3. The delineation was originally proposed by Jonsson (1966) and later adapted by Davies in the light of subsequent experimental findings. The hatched area depicts the region of applicability of Davies and

Villaret's (1999) model (DV99). Fig. 3 shows that the flow regime is transitional for the present tests except for two tests (Tests 13 and 14) where the flow regime was turbulent. This figure also allows a comparison between the present flow conditions and those of eight previous studies of wave-induced currents above rough flat beds or rippled beds. Sleath (1984) also measured drift velocities over a flat rough bed. These data are not shown in Fig. 3, however, the results reported were of the maximum near-bed drift rather than vertical profiles of the drift or the drift at the edge of the boundary layer. Jensen

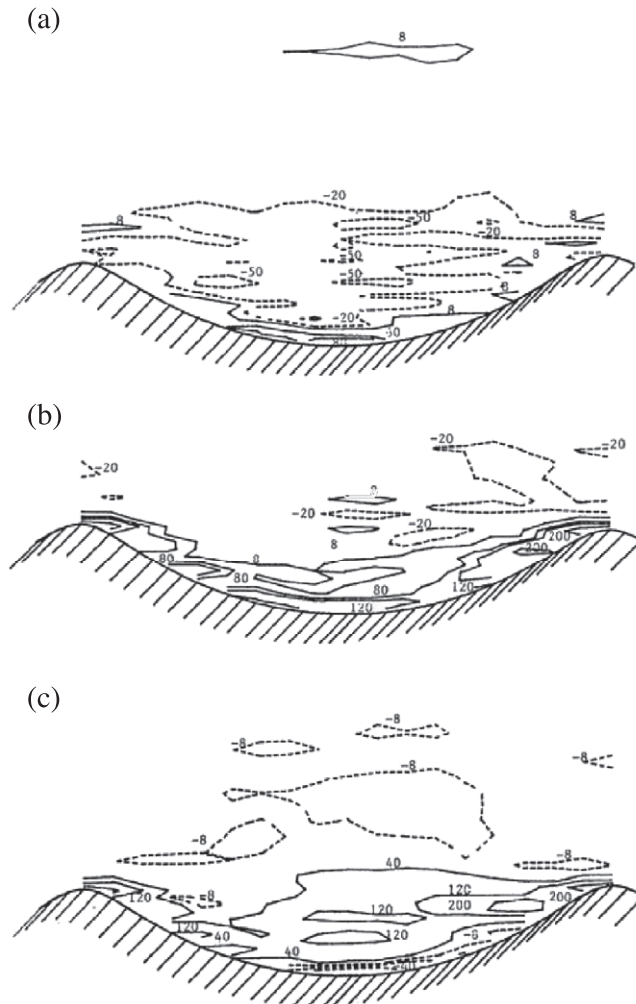


Fig. 7. Contours of the spanwise component of vorticity (rd/s). Test 2. (a) $\omega t = 1.01$, (b) $\omega t = 2.01$, (c) $\omega t = 3.02$, (d) $\omega t = 4.02$, (e) $\omega t = 5.03$, (f) $\omega t = 6.03$.

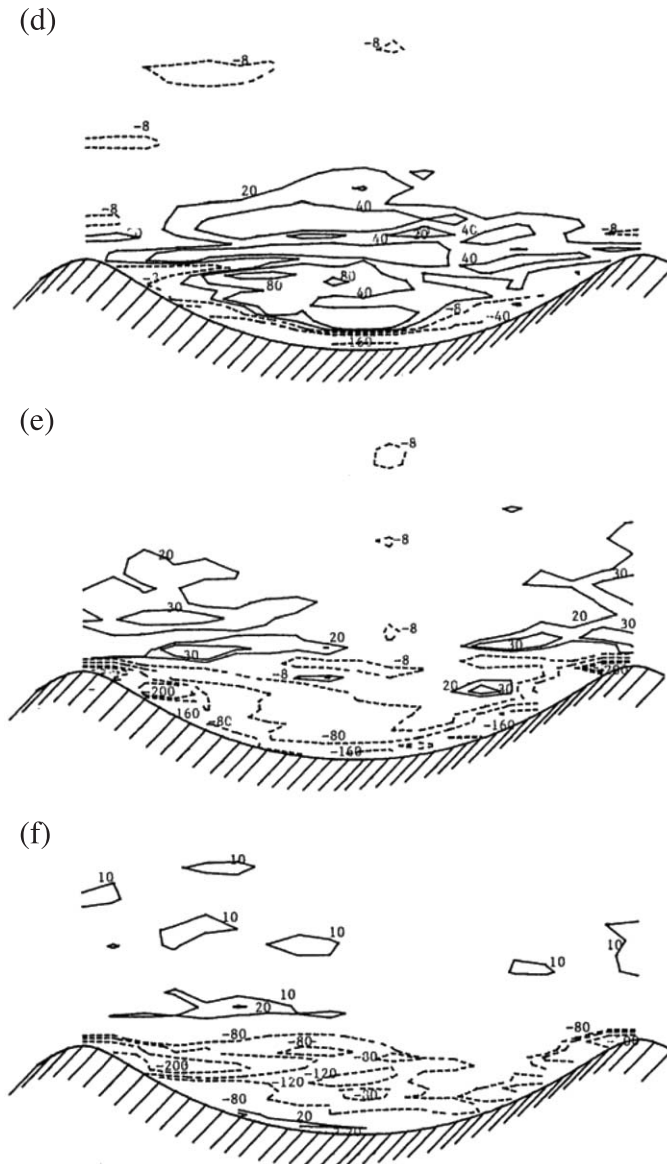


Fig. 7 (continued).

et al. (1989) analyzed in great detail turbulent oscillatory boundary-layer flows over both smooth and rough beds. They proposed a diagram illustrating the bed regimes: hydraulically smooth, transitional and rough.

Let us consider the eddy shedding process for present tests. If this process is the dominant momentum transfer process in the near-bed layer, the

approach adopted by DV99 ($a/k_s < 5$, turbulent flow regime) can be used to simulate present data and the applicability of the DV99 model in the transitional flow regime for the parameter ranges (in terms of R and a/k_s) involved can be assessed. Brebner et al. (1966) and Klopman (1994) made measurements above flat beds roughened with sand in the transitional flow regime. These measurements cannot be

simulated by the approach adopted by DV99 since they were obtained in the “upper” part of the transitional regime, involving greater values of a/k_s than for present tests. However, the data sets of Marin and Sleath (1994) and Ridler and Sleath (2000) are in the region of applicability of the DV99 model; for a same value of the Reynolds number, the values of a/k_s are lower than in the present experiments.

3. Eddy shedding

Distributions of the periodic component of the velocity vector are presented in Figs. 4 and 5 for Tests 1 and 2 at different times. The phase $\omega t=0$ where ω is the angular frequency ($\omega=2\pi/T$) and t is the time corresponds to the passage of the wave crest. The distributions of the velocity vectors show the formation of organized vortices each half-cycle on the leeside of ripples. The eddy shedding above ripple crests is clearly shown for Tests 1 and 2 by the contours of the spanwise component of vorticity Ω_p defined by $\Omega_p = \partial v_p / \partial x - \partial u_p / \partial y$ (Figs. 6 and 7). For Test 1 (Fig. 6), at $\omega t=1.26$, a vortex is about to be shed from the ripple’s crest and to be convected upstream. At $\omega t=2.26$, this vortex has just passed above the ripple’s crest. It will travel along the bed profile during about one half period for a distance of twice the wavelength of the

ripple. The counter-rotating vortex (positive vorticity in Fig. 6) has just been shed and passes above the ripple’s crest at $\omega t=5.28$; it will be convected downstream during the next half period. The same process of eddy shedding is observed for Test 2 (Fig. 7); in this case, the vortices tend to be flattened against the ripple profile owing to velocities which are greater than for Test 1. These results show evidence of eddy shedding despite the fact that present values of a/k_s are systematically larger (for a given value of the Reynolds number) than those considered in DV99, and that less coherent eddy shedding might have been expected at these larger values of a/k_s .

Fig. 8 shows that the horizontally averaged velocity $\langle u_p \rangle$ does not vary significantly with height for $y/k_s \geq 0.7$ when $\omega t=0$. The edge of the bottom boundary layer is considered for present tests to be at the height $y/k_s=1$.

4. Eddy viscosity

Momentum transfer in the near-bed layer is dominated for present tests in the case of transitional flow regime (with probably the exception of the two tests characterized by the smallest Reynolds numbers) by organized structures resulting from the shedding of vortices from ripple crests at flow reversal. The total shear stress τ_p is mainly due to periodic velocity

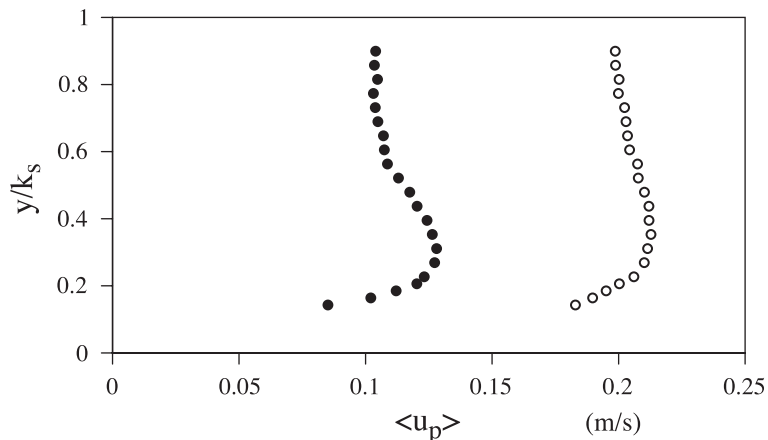


Fig. 8. Variation above the ripple’s crest of $\langle u_p \rangle$ with y/k_s when $\omega t=0$. Test 1 (solid circles) and Test 2 (open circles).

correlations (DV99): $\tau_p = -\rho \langle \tilde{u}_p \tilde{v}_p \rangle$ and it can be related to the horizontally averaged flow velocity gradient by:

$$\tau_p = \rho v_t \frac{\partial \langle u_p \rangle}{\partial y} \quad (8)$$

in which ρ is the fluid density. The evolutions during the course of the cycle of τ_p , of the horizontally averaged velocity gradient $\partial \langle u_p \rangle / \partial y$, of the velocity just outside the boundary layer u_0 and of the eddy viscosity v_t obtained from Eq. (8) are given in Figs. 9–11 for Test 1 and $y=4.2$ mm. The temporal evolution of τ_p (Fig. 9) displays several peaks which both confirm the need for a time-varying eddy viscosity, as pointed out in the turbulent flow regime above rippled beds by several investigators (see, for example, Sato et al., 1987 and Ikeda et al., 1991), and also indicate the presence of harmonics in that viscosity. The points for which the velocity gradient tends to be zero have not been plotted in Fig. 11 (temporal evolution of v_t). The times at which the peak values of v_t are obtained ($\omega t = 1.88$ and $\omega t = 4.90$ for Test 1) correspond to the time of eddy shedding. Fig. 11 also depicts the predicted temporal evolution of v_t according to the expression proposed by DV99:

$$v_t = \bar{v}_t (1 + \varepsilon_1 \exp(i\omega t) + \varepsilon_2 \exp(2i\omega t)) \quad (9)$$

in which \bar{v}_t is the period-averaged eddy viscosity, ε_1 and ε_2 complex coefficients: $\varepsilon_1 = |\varepsilon_1| \exp(i\varphi_1)$,

$\varepsilon_2 = |\varepsilon_2| \exp(i\varphi_2)$. The real part of v_t in Eq. (9) is given by:

$$Re(v_t) = \bar{v}_t [1 + |\varepsilon_1| \cos(\omega t + \varphi_1) + |\varepsilon_2| \cos(2\omega t + \varphi_2)], \quad (10)$$

and \bar{v}_t (also shown in Fig. 11) is estimated by using Nielsen's (1992) formula which applies for $a/k_s < 16.7$:

$$\bar{v}_t = 0.004 U_\infty k_s. \quad (11)$$

The phase angle φ_1 at which the main peak in v_t occurs during the cycle is defined by the following relation:

$$\varphi_1 = -\arccos \left(B - \frac{\overline{U_\infty}}{U_\infty} \right) \Delta\varphi \quad (12)$$

with $\Delta\varphi = 4^\circ$, $\varphi_2 = 2\pi + 2\varphi_1$, $\overline{U_\infty}$ being the drift at the edge of the boundary layer. Fig. 11 shows that the agreement between present data and the DV99 model is reasonably good; however, the asymmetry in the temporal evolution of v_t does not seem to be as strong as suggested by DV99. In other words, the value of $|\varepsilon_1|$, which governs the magnitude of this asymmetry, may be lower in the transitional flow regime than the value suggested by DV99 in the turbulent flow regime. By way of comparison, Fig. 11 also presents (DV99adj) the variation of v_t during the course of the cycle according to Eq. (10)

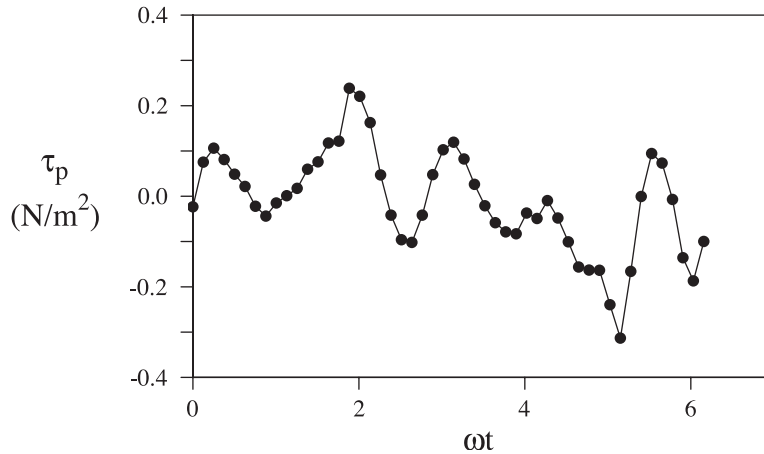


Fig. 9. Variation during the course of the cycle of the horizontally averaged shear stress τ_p . Test 1, $y=4.2$ mm.

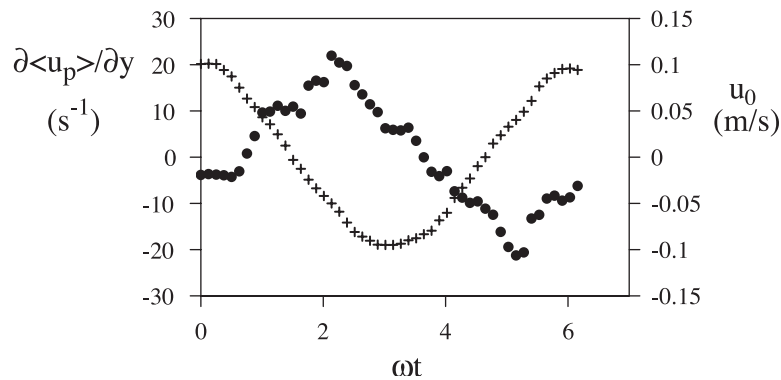


Fig. 10. Variation during the course of the cycle of the horizontally averaged velocity gradient at $y=4.2$ mm ($\partial\langle u_p\rangle/\partial y$, solid circles) and of the horizontal component of velocity just outside the bottom boundary layer (u_0 , pluses). Test 1.

but with the value of $|\varepsilon_1|$ proposed by DV99 ($|\varepsilon_1|=0.73$) reduced to $|\varepsilon_1|=0.30$, while maintaining the value of $|\varepsilon_2|$ proposed by DV99, that is $|\varepsilon_2|=1.3$. The effect of flow asymmetry being significant on the wave-induced currents, let us now consider the Eulerian drift close to the bed.

5. Eulerian drift

5.1. Vertical profiles of Eulerian drift

The measured vertical profiles of Eulerian drift \bar{U} , horizontally averaged over a ripple length, are depicted

in Fig. 12a and b for Tests 1 and 2, c being the wave-phase speed, with the profiles given by the Longuet-Higgins (1953), Nielsen (1992) and DV99 models. The upper edge of the bottom boundary layer ($y/k_s=1$) is high enough for the drift velocity not to vary any more with height above the bed. As mentioned by Mathisen and Madsen (1996b), the return flow in the channel develops itself a boundary layer and this leads to near-bed value of the return flow probably much smaller than the average value of depth. However, there may be a contribution from the return flow to the resulting streaming velocity measured in the present experiments. For the present data, the horizontal averaging below the ripple crest level in Fig. 12a and b was

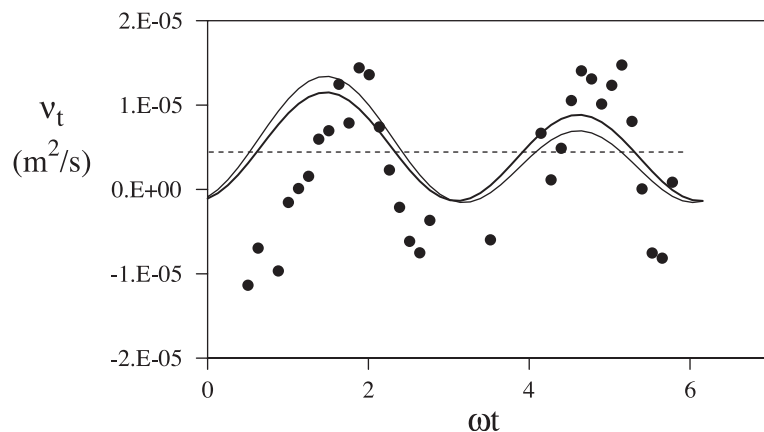


Fig. 11. Variation during the course of the cycle of the eddy viscosity. Test 1, $y=4.2$ mm. Present data (solid circles) are shown with Davies and Villaret's (1999) solution (DV99; thin solid line) and Davies and Villaret's "adjusted" solution (DV99adj; thick solid line). The value of the eddy viscosity (time-invariant) according to Nielsen's (1992) formula (Eq. (11)) is also displayed (thin dashed line).

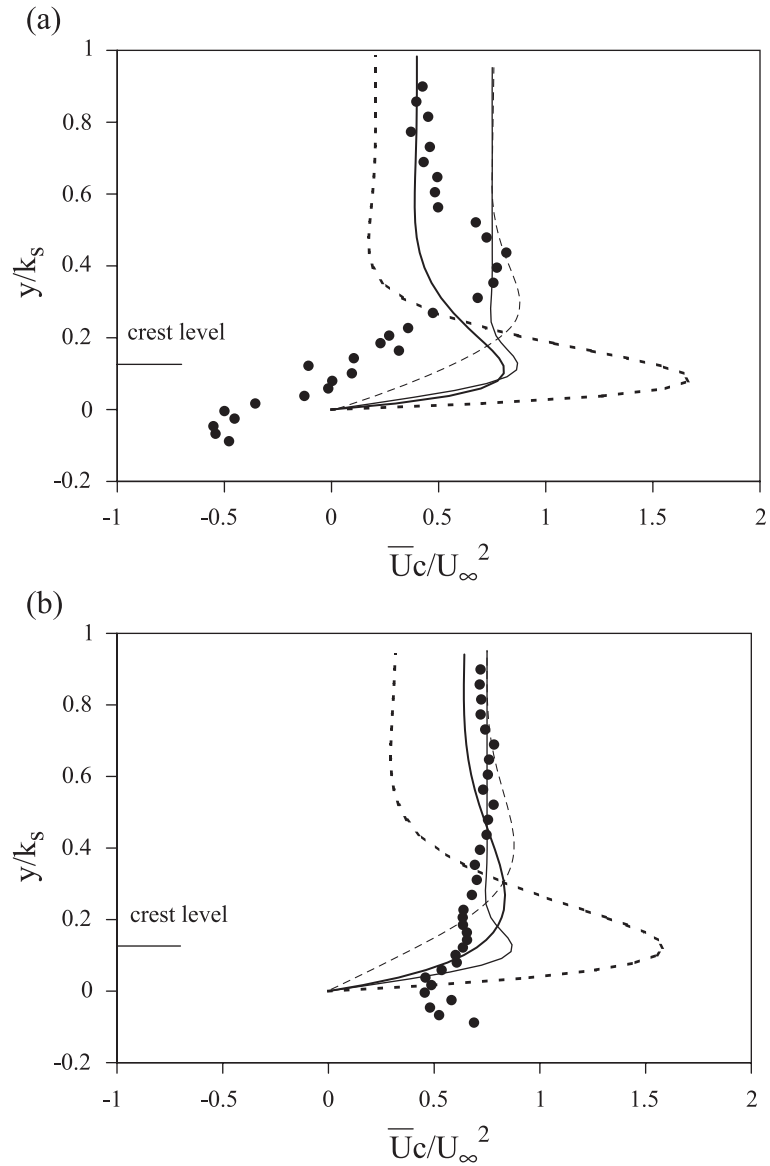


Fig. 12. Comparison between measured and predicted horizontally averaged drift profiles for Test 1 (a) and Test 2 (b). The solid circles indicate the measurements. The level of ripple crest is indicated by the solid line at the bottom left. The predicted profiles are from Longuet-Higgins' (1953) model (thin solid line), Nielsen's (1992) model (thin dashed line), Davies and Villaret's (1999) model (DV99, thick dashed line), and "adjusted" Davies and Villaret's model (DV99adj, thick solid line).

carried out over a length smaller than the ripple wavelength, the length of the fluid area below the ripple crest level decreasing for decreasing values of y . Longuet-Higgins' solution was obtained for a laminar flow above a smooth flat bed; in this case, k_s should be

interpreted as a numerical constant equal to 11.9 mm. Nielsen (1992) suggested to use the following formula:

$$\bar{U} = \int_0^y \frac{1}{v_t} \left(\frac{1}{\rho} \frac{\partial \bar{p}}{\partial x} y + \overline{u_p v_p} + \frac{1}{\rho} \overline{\tau_p(0)} \right) dy, \quad (13)$$

with

$$\overline{\rho(u_p v_p)} = -\rho \frac{1}{4} (a\omega)^2 k \delta [1 - e^{-\xi} (2\cos\xi - e^{-\xi} + 2\xi \sin\xi)], \quad (14)$$

where p is the pressure, $\tau_p(0)$ is the bed shear stress, v_t is a time-independent eddy viscosity given by Eq. (11), $\xi = y/\sqrt{2v_t/\omega}$, $\delta = 0.09\sqrt{k_s a}$, and with the assumptions of $\overline{\tau_p(0)} = -\rho(\overline{u_p v_p})_\infty$ and $\partial\overline{p}/\partial x = 0$. The overbar denotes time-averaging over one wave period. Fig. 12a and b shows that Nielsen's model gives the general trend of vertical profiles of Eulerian drift for Tests 1 and 2; however, the measured drift at the edge of the boundary layer appears to depend on the flow conditions and not to be fixed to the value $\overline{U_\infty}c/U_\infty^2 = 0.75$ corresponding to a laminar flow above a smooth bed (Longuet-Higgins, 1953). This point will be further considered in the following section. The solution of the DV99 model is given by:

$$\begin{aligned} \overline{U} = \overline{U}_s & \left[1 + \frac{1}{2} |\varepsilon_2| \cos(\varphi_2) \right] \\ & + \frac{U_\infty |\varepsilon_1|}{2} [\exp(-\alpha y) \cos(\alpha y + \varphi_1) - \cos(\varphi_1)] \\ & + \frac{|\varepsilon_2| U_\infty^2}{4c} \left\{ \exp(-\alpha y) \cos(\alpha y + \varphi_2) \right. \\ & + \alpha y \exp(-\alpha y) [\cos(\alpha y + \varphi_2) + \sin(\alpha y + \varphi_2)] \\ & \left. - \exp(-\sqrt{2}\alpha y) \cos(\sqrt{2}\alpha y + \varphi_2) \right\} + \frac{|\varepsilon_2| BU_\infty}{2} \\ & \times [\exp(-\sqrt{2}\alpha y) \cos(\sqrt{2}\alpha y + \varphi_2) - \cos(\varphi_2)] \end{aligned} \quad (15)$$

where \overline{U}_s is the basic Stokes' contribution to the Eulerian drift and $\alpha = (\phi/\sqrt{v_t}T)^{1/2}$. The DV99 model does not seem to be directly applicable to the transitional flow regime since the measurements do not show a strong near-bed jet in the direction of wave advance and since the Eulerian drift is underestimated by the analytical model for $y/k_s \geq 0.4$. However, a reduction in the model coefficient $|\varepsilon_1|$ significantly improves the estimation of the vertical profile of drift, as shown for Test 1 in Fig. 12a by the "adjusted" model (DV99adj) for which $|\varepsilon_1| = 0.3$ (and $|\varepsilon_2| = 1.3$). For this test, the drift shows a maximum in the direction of wave

propagation at a value of y/k_s equal to about 0.45. The value of this maximum (approximately equal to $2\overline{U_\infty}$) and the drift far from the bed ($y/k_s \geq 0.7$) are well reproduced by the adjusted model; the height at which the maximum occurs is nevertheless underestimated. For Test 2, a reduction in both coefficients $|\varepsilon_1|$ and $|\varepsilon_2|$ improves the overall fit to the data. The contours of the spanwise component of vorticity have shown for this test that the vortices tend to be flattened against the ripple profile. This leads to a variation of the eddy viscosity v_t throughout the wave cycle less significant than for Test 1, and consequently to a lower value of $|\varepsilon_2|$. The experimental data for Test 2 appear to be in reasonable agreement with the analytical model by reducing the value of $|\varepsilon_2|$ proposed by DV99 in the turbulent flow regime from $|\varepsilon_2| = 1.3$ to $|\varepsilon_2| = 0.3$ and by keeping the same value of $|\varepsilon_1|$ as for Test 1 ($|\varepsilon_1| = 0.3$) in contrast to the DV99 suggested value of $|\varepsilon_1| = 1.25$ (Fig. 12b, Test 2, DV99adj).

Assuming in the transitional flow regime for the parameter ranges (in terms of R and a/k_s) involved for Tests 1 and 2 a constant value of $|\varepsilon_1|$:

$$|\varepsilon_2| = 0.3 \quad (16a)$$

and a linear variation of the coefficient $|\varepsilon_1|$ with the Reynolds number R , the value of $|\varepsilon_2|$ may be estimated by the following equation:

$$|\varepsilon_2| = 1.69 - 2.6 \times 10^{-4} R. \quad (16b)$$

In order to more accurately estimate the region of validity of these adjusted values of the coefficients $|\varepsilon_1|$ and $|\varepsilon_2|$, let us consider the Eulerian drift at the edge of the boundary layer for Tests 1–12.

5.2. The drift at the edge of the boundary layer

The variation of $\overline{U_\infty}c/U_\infty^2$ with R in the transitional flow regime is displayed in Fig. 13. The symbols for present tests (solid circles) have been linked with solid lines to facilitate comparison with the other data sets. Since Brebner et al. (1966) measured the drift using fluorescent tracers and neutrally buoyant beads, they refer to the Lagrangian velocity rather than the Eulerian drift. For this reason, the appropriate near-bed Stokes drift has been subtracted from the measured values in order to be able to compare these data with

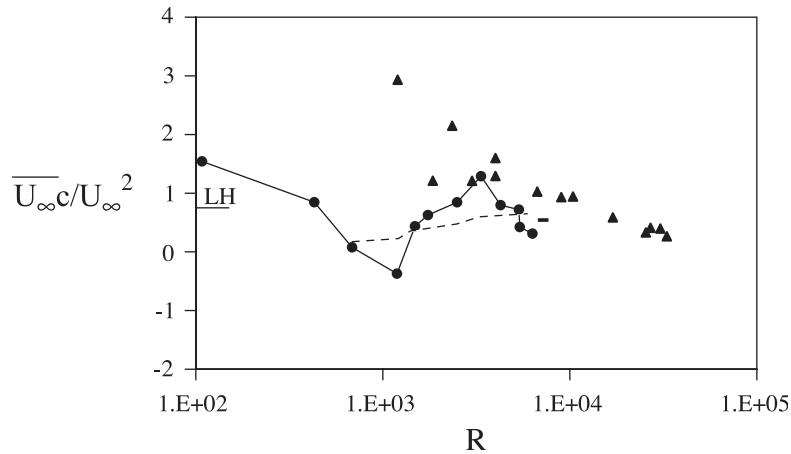


Fig. 13. Nondimensional Eulerian drift at the edge of the boundary layer in relation to R (Tests 1–12). The symbols representing the various data sets are as defined in Fig. 3. Davies and Villaret's (1999) "adjusted" solution (DV99adj; thin dashed line) is shown with Longuet-Higgins' (1953) solution (solid line labelled LH).

the other Eulerian data sets in Fig. 13. The drift at the edge of the boundary layer for present tests is in the direction of wave propagation (except for one test where the drift is slightly negative), whereas this drift is oriented in the opposite direction in the turbulent flow regime (DV99). The wave-induced currents obtained by Brebner et al. (1966) and Klopman (1994) exhibit greater values than for present tests in the whole range of R plotted in Fig. 13. As previously pointed out (Section 2.3), these measurements cannot be simulated by the DV99 model since they involve high values of a/k_s . The effect of wave asymmetry, which is greater when a/k_s takes low values, is to favour drift in the direction opposite to that of wave propagation. It is therefore not surprising that present data lie below the Brebner et al. and Klopman data in Fig. 13. Measurements of wave-induced currents above rough flat beds or rippled beds have also been carried out by Van Doorn and Godefroy (1978), Villaret and Perrier (1992), Marin and Sleath (1994), Mathisen and Madsen (1996b), Fredsøe et al. (1999), and Ridler and Sleath (2000). These data are not shown in Fig. 13 since they are in the region of applicability of the DV99 model (Fig. 3). Fig. 13 also depicts the results of the DV99 model for the present tests (except for the two tests with the smallest Reynolds numbers) using the adjusted values of the coefficients $|\varepsilon_1|$ and $|\varepsilon_2|$ (DV99adj). At the edge of

the boundary layer, the solution of the DV99 model (Eq. (15)) becomes simply:

$$\frac{\overline{U_\infty c}}{U_\infty^2} = \frac{3}{4} \left[1 + \frac{1}{2} |\varepsilon_2| \cos(\varphi_2) \right] - \frac{1}{2} \frac{c}{U_\infty} |\varepsilon_1| \cos(\varphi_1) - \frac{1}{2} B \frac{c}{U_\infty} |\varepsilon_2| \cos(\varphi_2). \quad (17)$$

The solution of the adjusted model (DV99adj) appears to be in reasonable agreement with present data. This suggests that the DV99 model can be applied in the transitional flow regime using the adjusted values of the coefficients $|\varepsilon_1|$ and $|\varepsilon_2|$ (Eq. (16a,b)) when $1000 \leq R \leq 6500$ for values of a/k_s varying from 1 for the lower Reynolds numbers to 3 for the larger Reynolds numbers.

When the asymmetry in the flow is very weak ($B < 0.01$; Test 3, lowest value of R), the effect of bed roughness is to increase the drift in the direction of wave propagation, as mentioned by Sleath (1974b) in the transitional flow regime. Present data show a minimum for the drift when $R \approx 1000$; this may be due for present tests involving a fixed rippled bed to the vortices which are flattened when R increases beyond this value (Section 3).

6. Conclusions

Laser-Doppler anemometer measurements have been made in a laboratory flume with a fixed rippled bed under weakly asymmetrical waves ($B < 0.1$) to analyze the wave-induced Eulerian drift in the bottom boundary layer in the transitional flow regime. The momentum transfer is dominated by eddy shedding through the parameter ranges in which the data were obtained. Davies and Villaret's (1999) model (DV99), which has been developed for the estimation of the Eulerian drift above rippled and very rough beds ($a/k_s < 5$) in the turbulent flow regime, cannot be used directly in the transitional flow regime. However, the region of validity of the DV99 model can be extended to the "lower" part of the transitional flow regime in the parameter ranges $1000 \leq R \leq 6500$ and $1 \leq a/k_s \leq 3$ by using adjusted values (Eq. (16a,b)) of the coefficients which represent the variation in amplitude of the eddy viscosity ν_t at the first harmonic frequency (result of asymmetry in the free-stream flow) and at the second harmonic frequency (result of eddy shedding from the bed). The Eulerian drift at the edge of the boundary layer is oriented in the direction of wave propagation in these parameter ranges, while it is oriented in the opposite direction in the turbulent flow regime (DV99).

Acknowledgements

The author gratefully acknowledges Dr. Alan G. Davies for very useful comments.

References

- Bijker, E.W., Kalkwijk, J.P.T., Pieters, T., 1974. Mass transport in gravity waves on a sloping bottom. Proc. 14th Int. Conf. on Coastal Eng., ASCE, Copenhagen, 447–465.
- Block, M.E., Davies, A.G., Villaret, C., 1994. Suspension of sand in oscillatory flow above ripples: discrete vortex model and laboratory experiments. In: Belorgey, M., Rajaona, R.D., Sleath, J.F.A. (Eds.), *Sediment Transport Mechanisms in Coastal Environments and Rivers*. World Scientific, Singapore, pp. 246–254.
- Brebnar, A., Askew, J.A., Law, S.W., 1966. The effect of roughness on the mass-transport of progressive gravity waves. Proc. 10th Int. Conf. on Coastal Eng., ASCE, Tokyo, 175–184.
- Brøker, I., 1985. Wave-generated ripples and resulting sediment transport in waves. Series paper No. 36, Inst. of Hydrodynamics and Hydraulic Engineering, ISVA, Techn. Univ. of Denmark.
- Collins, J.I., 1963. Inception of turbulence at the bed under periodic gravity waves. J. Geophys. Res. 68 (21), 6007–6014.
- Davies, A.G., 1980. Field observations of the threshold of sand motion in a transitional wave boundary layer. Coast. Eng. 4, 23–46.
- Davies, A.G., Villaret, C., 1998. Wave-induced currents above rippled beds and their effects on sediment transport. In: Dronkers, J., Scheffers, M. (Eds.), *Physics of Estuaries and Coastal Seas*. Balkema, Brookfield, VT, pp. 187–199.
- Davies, A.G., Villaret, C., 1999. Eulerian drift induced by progressive waves above rippled and very rough beds. J. Geophys. Res. 104 (C1), 1465–1488.
- Fredsøe, J., Sumer, B.M., Laursen, T.S., Petersen, C., 1993. Experimental investigation of wave boundary layers with a sudden change in roughness. J. Fluid Mech. 252, 117–145.
- Fredsøe, J., Andersen, K.H., Sumer, B.M., 1999. Wave plus current over a ripple-covered bed. Coast. Eng. 38, 177–221.
- Hansen, E.A., Fredsøe, J., Deigaard, R., 1994. Distribution of suspended sediment over wave-generated ripples. J. Waterw. Port, Coast., Ocean Eng. 120 (1), 37–55.
- Hsu, T.-W., Ou, S.-H., 1994. On the mass transport of water waves in a turbulent boundary layer. Ocean Eng. 21 (2), 195–206.
- Huang, C.J., Dong, C.M., 2002. Propagation of water waves over rigid rippled beds. J. Waterw. Port, Coast. Ocean Eng. 128 (5), 190–201.
- Ikeda, S., Horikawa, K., Nakamura, H., Noguchi, K., 1991. Oscillatory boundary layer over a sand ripple model. Coast. Eng. Jpn. 34 (1), 15–29.
- Jacobs, S.J., 1984. Mass transport in a turbulent boundary layer under a progressive water wave. J. Fluid Mech. 146, 303–312.
- Jensen, B.L., Sumer, B.M., Fredsøe, J., 1989. Turbulent oscillatory boundary layers at high Reynolds numbers. J. Fluid Mech. 206, 265–297.
- Johns, B., 1970. On the mass transport induced by oscillatory flow in a turbulent boundary layer. J. Fluid Mech. 43, 177–185.
- Jonsson, I.G., 1966. Wave boundary-layers and friction factors. Proc. 10th Int. Conf. on Coastal Eng., ASCE, Tokyo, 127–148.
- Klopman, G., 1994. Vertical structure of the flow due to waves and currents. Rep. H840.30, Part II, Delft Hydraulics, Delft.
- Liu, P.L.-F., Davis, M.H., Downing, S., 1996. Wave-induced boundary layer flows above and in a permeable bed. J. Fluid Mech. 325, 195–218.
- Longuet-Higgins, M.S., 1953. Mass transport in water waves. Philos. Trans. R. Soc. Lond., A 245 (903), 535–581.
- Longuet-Higgins, M.S., 1958. The mechanics of the boundary-layer near the bottom in a progressive wave. Proc. 6th Int. Conf. on Coastal Eng., ASCE, Miami, 184–193.
- Marin, F., Sleath, J.F.A., 1994. Mass transport over rippled beds. In: Belorgey, M., Rajaona, R.D., Sleath, J.F.A. (Eds.), *Sediment Transport Mechanisms in Coastal Environments and Rivers*. World Scientific, Singapore, pp. 246–254.
- Mathisen, P.P., Madsen, O.S., 1996a. Waves and currents over a fixed rippled bed: 1. Bottom roughness experienced by waves in

- the presence and absence of currents. *J. Geophys. Res.* 101 (C7), 16533–16542.
- Mathisen, P.P., Madsen, O.S., 1996b. Waves and currents over a fixed rippled bed: 2. Bottom and apparent roughness experienced by currents in the presence of waves. *J. Geophys. Res.* 101 (C7), 16543–16550.
- Nakato, T., Locher, F.A., Glover, J.R., Kennedy, J.F., 1977. Wave entrainment of sediment from rippled beds. *J. Waterw. Port. Coast. Ocean Eng.* 103 (WW1), 83–99.
- Nielsen, P., 1992. Coastal bottom boundary layers and sediment transport. *Advanced Series on Ocean Engineering*, vol. 4. World Scientific, Singapore.
- O'Hare, T.J., 1992. Sand-bar evolution beneath partially standing waves. PhD thesis. University of Wales.
- Ribberink, J.S., Al-Salem, A.A., 1995. Sheet flow and suspension of sand in oscillatory boundary layers. *Coast. Eng.* 25, 205–225.
- Ridler, E.L., Sleath, J.F.A., 2000. Effect of bed roughness on time-mean drift induced by waves. *J. Waterw. Port. Coast. Ocean Eng.* 126 (1), 23–29.
- Sato, S., Shimosako, K., Watanabe, A., 1987. Measurements of oscillatory turbulent boundary layer flow above ripples with a laser-Doppler velocimeter. *Coast. Eng. Jpn.* 30 (1), 89–98.
- Scandura, P., Vittori, G., Blondeaux, P., 2000. Three-dimensional oscillatory flow over steep ripples. *J. Fluid Mech.* 412, 355–378.
- Sleath, J.F.A., 1974a. Mass transport over a rough bed. *J. Mar. Res.* 32 (1), 13–24.
- Sleath, J.F.A., 1974b. A numerical study of the influence of bottom roughness on mass transport by water waves. In: Brebbia, C.A., Connor, J.J. (Eds.), *Numerical Methods in Fluid Dynamics*. Pentech Press, London, pp. 482–493.
- Sleath, J.F.A., 1984. Measurements of mass transport over a rough bed. *Proc. 19th Int. Conf. on Coastal Eng., ASCE*, Houston, Texas, 1149–1160.
- Swart, D.H., 1976. Coastal sediment transport. Computation of longshore transport. Rep. R968: Part I. Delft Hydraulics, Delft.
- Trowbridge, J.H., Madsen, O.S., 1984. Turbulent wave boundary layers: 2. Second-order theory and mass transport. *J. Geophys. Res.* 89 (C5), 7999–8007.
- Trowbridge, J.H., Kanetkar, C.N., Wu, N.T., 1986. Numerical simulation of turbulent wave boundary layers. *Proc. 20th Int. Conf. on Coastal Eng., ASCE*, Taipei, 1623–1637.
- Van Doorn, T., Godefroy, H.W.H.E., 1978. Experimental investigation of the bottom boundary layer under periodic progressive water waves. Rep. M1362: Part I. Delft Hydraulics, Delft.
- Villaret, C., Perrier, G., 1992. Transport of fine sand by combined waves and current: an experimental study. Rep. HE-42/92.68, Electr. de France, Chatou.
- Vittori, G., Blondeaux, P., 1996. Mass transport under sea waves propagating over a rippled bed. *J. Fluid Mech.* 314, 247–265.